

Supporting Information

Friction heat-driven robust self-lubricity of *n*-alkanols/EP coatings enabled by solid-liquid phase transition

Hao Li, ^{*a} Cheng Cao,^a Yuting Li,^a Xiaoqiang Fan,^a Junhui Sun, ^{*b,c} and Minhao Zhu ^{a,b}

^aKey Laboratory of Advanced Technologies of Materials (Ministry of Education), School of Materials Science and Engineering, Southwest Jiaotong University, Chengdu 610031, China.

^bTribology Research Institute, School of Mechanical Engineering, Southwest Jiaotong University, Chengdu 610031, China.

^cState Key Laboratory of Solid Lubrication, Lanzhou Institute of Chemical Physics, Chinese Academy of Sciences, Lanzhou 730000, China.

*Corresponding authors:

Hao Li (E-mail: lihao@swjtu.edu.cn)

Junhui Sun (E-mail: junhuisun@swjtu.edu.cn)

Results

1. Morphology of *n*-alkanols and *n*-alkanols/EP coatings

Fig. S1 shows molecular formula and SEM images of different kinds of *n*-alkanols. 1-hexadecanol (HD), octadecyl alcohol (OD) and 1-docosanol (DS) are labeled with different alkyl chain lengths, among which the alkyl chain of HD is the shortest, and the alkyl chain of DS is the longest. There are a lot of micropores on the surface of HD powder and OD powder, but there are no micropores on the surface of DS powder. The micropores on the surface of HD powder are larger and denser, which provides conditions for mechanical interlocking between HD and EP.

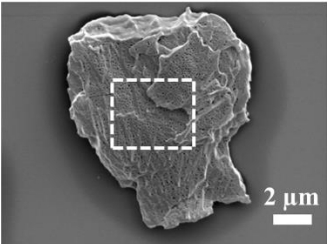
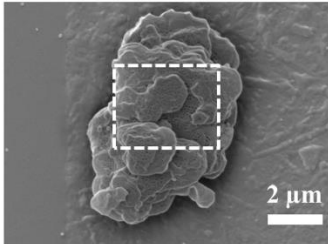
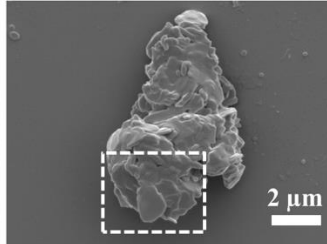
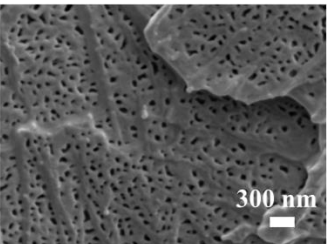
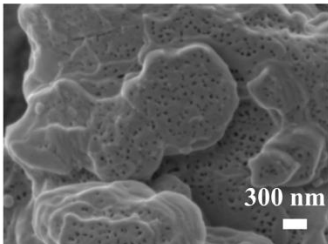
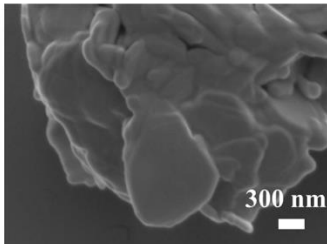
	HD	OD	DS
Molecular formula	$\text{CH}_3(\text{CH}_2)_{15}\text{OH}$	$\text{CH}_3(\text{CH}_2)_{17}\text{OH}$	$\text{CH}_3(\text{CH}_2)_{21}\text{OH}$
Micro-morphology			
			

Fig. S1 Molecular formula and SEM images of different kinds of *n*-alkanols.

Surface roughness and cross-section morphology of coatings are shown in Fig. S2. The surface roughness of pure EP coating is smaller than other OD/EP coatings, while the surface roughness of the OD/EP coatings increases gradually with the increase of the content, and agglomeration occurs when the content of OD is 24 wt.%. Among the composite coatings with different kinds of *n*-alkanols added at the same molar ratio (Fig. 1B), HD/EP coating has the lowest surface roughness, and no obvious agglomeration is found for the coating.

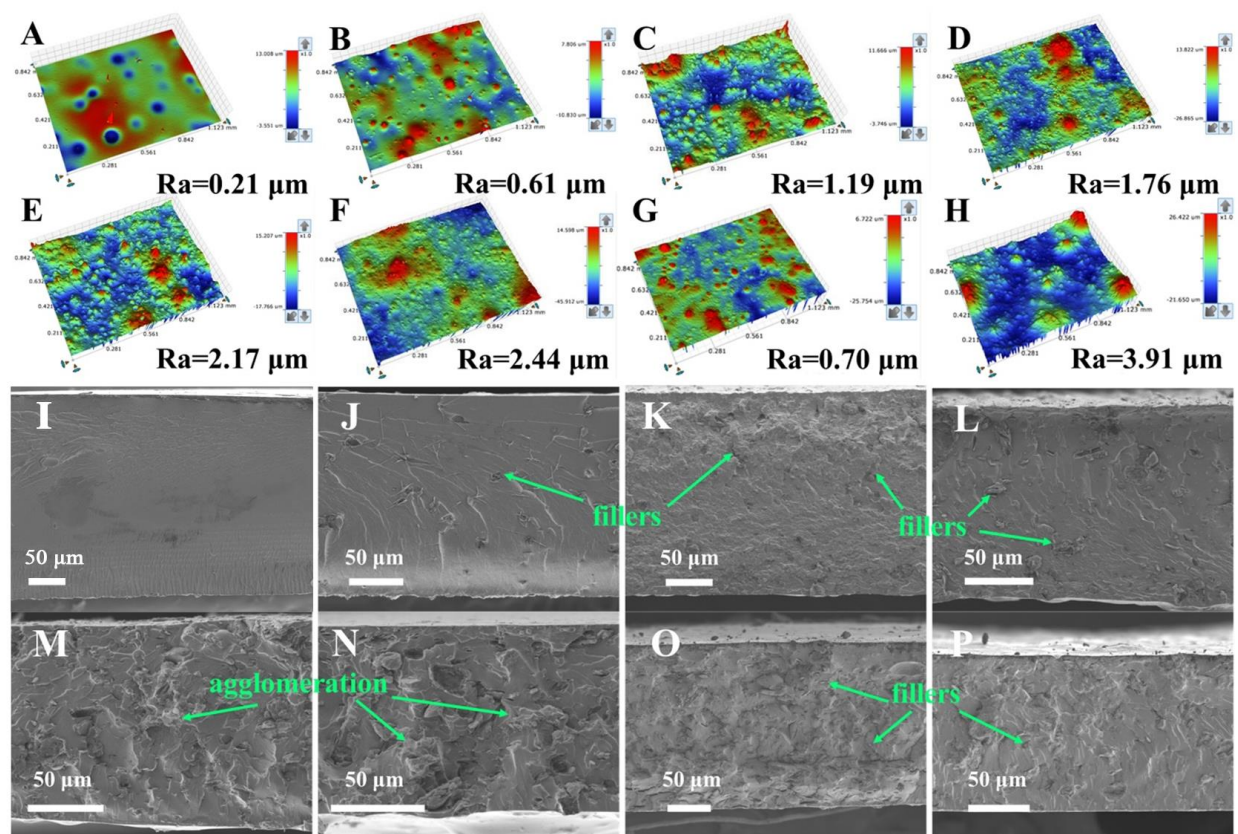


Fig. S2 Surface roughness and cross-section morphology of coatings (A, I) Pure EP; (B, J) 4 wt.%; (C, K) 10 wt.%; (D, L) 16 wt.%; (E, M) 24 wt.%; (F, N) 30 wt.%; (G, O) HD/EP; (H, P) DS/EP.

2. Phase transition points of *n*-alkanols and *n*-alkanols/EP coatings

Table S1 indicates that the melting point of *n*-alkanols increases with the increase of alkyl chain length, and the melting point of the *n*-alkanols added to the coating changes slightly.

Table S1. Phase transition results of *n*-alkanols and *n*-alkanols/EP coating from DSC curves.

Samples	Melting process	
	T _m (°C)	ΔH _m (J/g)
HD	49.5	206.4
OD	59.3	200.0
DS	68.5	152.3
Pure EP	-	-
HD/EP	50.9	15.3
OD/EP	58.2	29.9
DS/EP	69.3	20.1

3. Structure of the *n*-alkanols/EP coatings

The sharp diffraction peaks in XRD (Fig. S3) show that HD, OD and DS in the composite coating still have good crystallization ability. Accordingly, the grain sizes of HD, OD and DS particles inner the composite coatings were calculated via the XRD peak using Debye Scherrer,¹ and the calculated grain sizes are 30 nm, 37 nm and 21 nm respectively (Table S2).

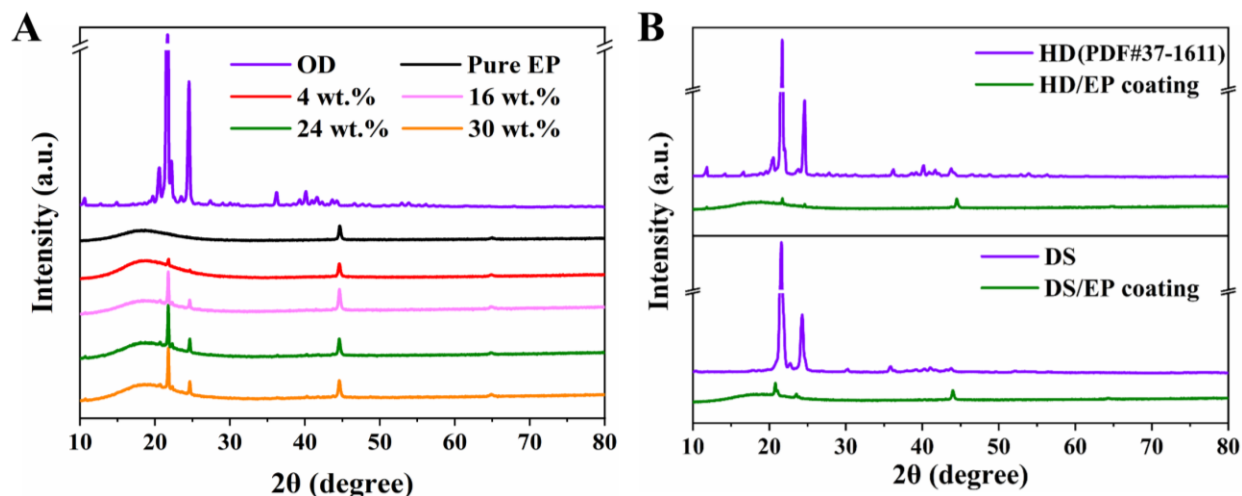


Fig. S3 XRD curves of (A) HD, EP and OD/EP coatings and (B)DS, DS, HD/EP coatings and DS/EP coating.

Table S2. Grain sizes of different *n*-alkanols

Samples	Grain sizes (nm)
HD	~30
OD	~37
DS	~21

4. Mechanical and thermal stability of the *n*-alkanols/EP coatings

Dynamic mechanical thermal analysis (DMA) has been widely employed for studying the molecular structures, thermo-mechanical properties, interfacial characteristics and viscoelastic behaviors of polymers and polymer composites.² The dynamic storage modulus (E') and the mechanical loss factor $\tan\delta$ are presented in Fig. S4, respectively, for the Pure EP, HD/EP, OD/EP and DS/EP composite coatings as a function of temperature from -40 to 90 °C.

At room temperature (25 °C), the E' increases with increased OD content, reaching a maximum value of 1743 MPa when the OD content is 16 wt.%, and then E' decreased with further increase of OD. (Fig. S4 A and Table S3). First of all, it should be noted that the variation of E' is not determined by the chemical reaction E' between OD and EP, as the reaction could only be carried out under high temperature and catalyst, which is proved by FTIR analysis. The infrared results in Fig. 3D indicates that the infrared peaks of the OD/EP coating with OD content of 16 wt.% and pure EP coating are basically the same, indicating that there is no chemical reaction between OD and EP. Therefore, there is only a simple mechanical and physical interaction between OD and EP.³ Through the characterization of the cross-section morphology on the coating and the micro-morphology of OD powder, it is found that the change of E' is mainly affected by two factors. On the one hand, as the OD content increased, the roughness of coating cross-section increases, and obvious agglomeration occurs when the OD content is 24 wt.% (Fig. S2). Therefore, the addition of OD would damage the crosslinking density of EP and reduce the E' of the coating.^{4,5} Moreover, the OD as a flexible filler would also reduce the E' of the coating. On the other hand, the mechanical interaction between OD and EP effects the E' . A large number of micropores are distributed on the surface of OD powder, which provides conditions for the mechanical interlocking between OD and EP,⁶ so as to improve the E' of the coating (Fig. S1). The excellent interfacial compatibility between OD and EP also proves the existence of mechanical interlocking (Fig. S2). Therefore, the variation of E' is due to a competitive mechanism.

It is discovered that the E' of HD/EP coating is the highest at room temperature (Fig. S4 C and Table S3) as compared with other *n*-alkanols/EP composite coatings, owing to the larger and denser micropores in HD powder, resulting in a stronger mechanical interlocking effect.

The loss factor curve is shown in Fig. S4 B and D. It could be seen that pure EP and blend system have obvious glass transition, and the temperatures of maximum loss factor (T_g) are almost

identical to the melting point of the blends observed in the DSC results (Fig. 1D), indicating that the loss spectra encompass the phase transition.⁷

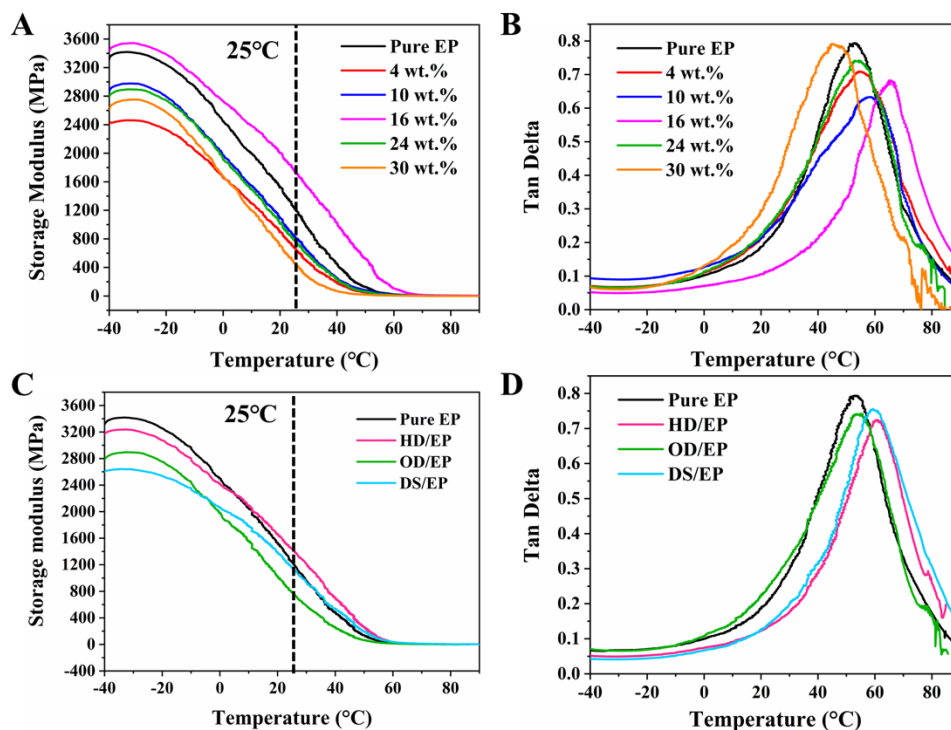


Fig. S4 Dynamic mechanical thermal analysis of coating. (A, B) Dynamic storage modulus and viscoelastic loss factor of OD/EP composite coatings with different content of OD. (C, D) Dynamic storage modulus and viscoelastic loss factor of *n*-alkanols/EP composite coatings.

Table S3. DMA analysis data

DMA characteristic	Different kinds of epoxy coatings							
	Pure EP	OD/EP					HD/EP	DS/EP
		4 wt.%	10 wt.%	16 wt.%	24 wt.%	30 wt.%		
Storage Modulus at 25 °C (MPa)	1247	655	792	1743	790	430	1441	1158
Glass transition temperature (°C)	52.9	55.3	58.1	65.1	54.1	45.5	60.8	59.8

The thermal stability of pure EP coating and OD/EP composite coating was studied by TGA. TGA curves of samples are shown in Fig. S5, and the detailed thermal decomposition data are

listed in Table S4. In Fig. S5, the pristine OD and pure EP shows one-stage decomposition mechanism. The onset degradation temperature of pristine OD and pure EP coating are 203.9 °C and 276.0 °C respectively. This result indicates that OD and pure EP coating have homogeneous chemical structure. Different from pristine OD and pure EP, the OD/EP coatings show two-stage thermal decomposition behaviors. This is because OD and pure EP have different decomposition temperature zones, which are 185-280 °C and 290-452 °C respectively. The first stage is chain degradation of OD, and the second stage is chain degradation of pure EP. The results of TGA show that the addition of OD to EP can stabilize the thermal decomposition performance of OD. In addition, the thermal degradation temperature of all coatings can be stabilized at 200 °C, which proves that the composite coatings have good thermal stability.

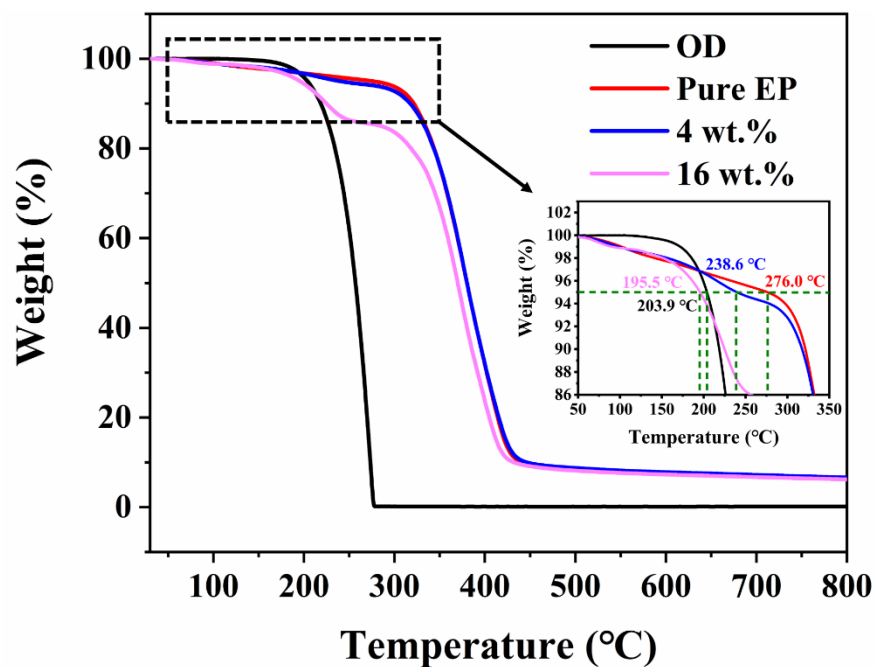


Fig. S5 TGA curves of pristine OD, pure EP and OD/EP coatings with different OD content.

Table S4. Decomposition data of pristine OD, pure EP and OD/EP coating with different OD content form TGA curves.

Samples	T _{-5%}	T _{-max}		CR (%)
		First step	Second step	
OD	203.9	274.2	-	0.14%
Pure EP	276.0	-	377.7	6.45%
4 wt. %	238.6	215.9	375.4	6.71%
16 wt. %	195.5	226.0	371.2	6.28%

The dynamic property of the HD/EP coating was evaluated by scratch repairing test. According to Fig. S6, an artificial scratch was observed using optical microscope after self-healing process at 70 °C for a predetermined time. Result shows that the HD/EP coating has great self-healing properties at 70 °C. The scratch disappeared gradually and can hardly be seen after 90 s.

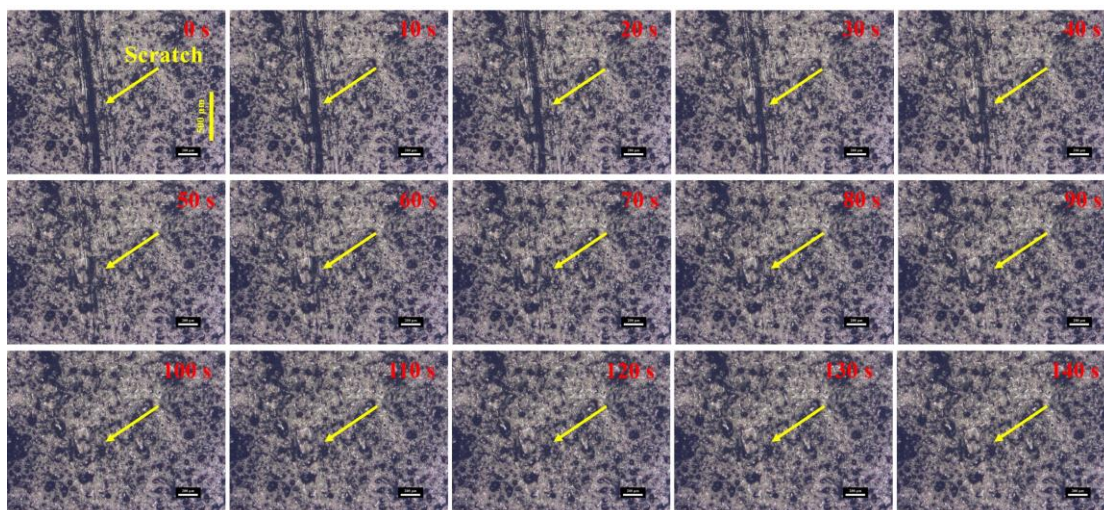


Fig. S6 Optical microscope photographs of the HD/EP coating taken during scratch healing test.

5. Tribological performance of the *n*-alkanols/EP coatings

The friction testing machine with ball-on-disk configuration was built independently by the laboratory (Fig. S7 A), and the form of friction is rotation (Fig. S7 B).

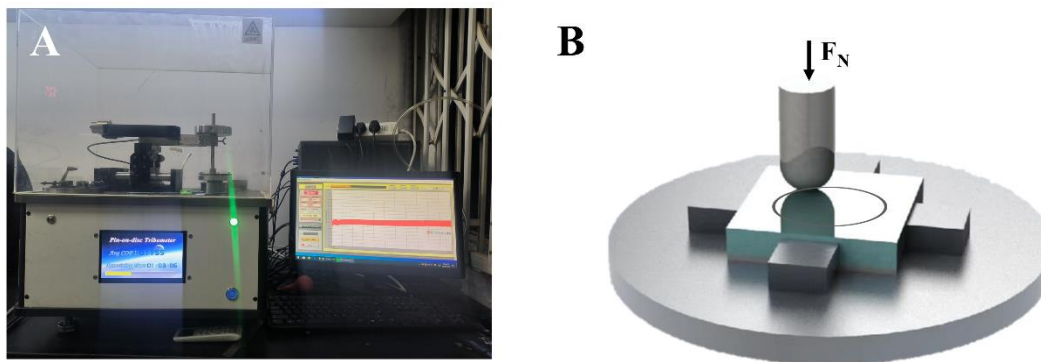


Fig. S7 The actual photograph of the tribo-tester along with the schematic diagram. (A) Actual photograph of the tribo-tester. (B) Schematic diagrams of the friction experiments.

Fig. S8 presents the relationship between the friction properties of OD/EP and the OD contents under different sliding speeds (100 rpm, 500 rpm). The friction coefficients of pure EP coating are the maximum under the two sliding speeds, which decrease with the increase of OD content. As for the OD/EP coatings with 24 wt.% OD, the friction coefficients are as low as 0.124 and 0.119 under 100 rpm and 500 rpm, respectively (Fig. S8 B). It is inferred that, the phase transition of OD in the friction process follows by the lubricant flowing out, resulting in the formation of a lubricant film at the interface. When the OD content further increases to 30 wt.%, the friction coefficient remains stable, indicating that a continuous liquid lubricant layer is formed when the OD content is higher than 16 wt.%. In addition, the friction coefficients at high speed are smaller than that at low speed, which is due to the fact that more friction heat is generated at high speed to induce abundant liquid lubricant.^{8,9}

The wear rates of OD/EP coating after friction tests are presented in Fig. S8 C. After the incorporation of OD, the wear rates of the OD/EP coatings are greatly decreased. Compared to pure EP coating, the wear rate of the OD/EP coating with 24 wt.% OD is lowered by 95.9% and 97.5% under 100 rpm and 500 rpm, respectively. Intriguingly, with the increased of OD content, the wear rates at various sliding speeds represent different relativity. When the content of OD is less than 10 wt.%, the wear rate at 500 rpm is higher than that at 100rpm. As the OD content is

higher than 10 wt.%, the wear rate at 500 rpm gets lower than those at 100rpm (Fig. S8 C). The variation in wear rate is mainly due to the result of a pair of competition mechanisms caused by high speed. The friction heat generated at high speed will not only lead to softening of coating, which could deteriorate wear of coating,^{8,10,11} but also stimulates liquid lubricants to reduce wear.⁹ Therefore, when the content of OD is less than 10 wt.%, the negative factor of coating softening is dominant, resulting in high wear rate at high speed. With further increasing OD content, the positive factor of producing more liquid lubricant plays a determinant role in decreasing the wear rate at high speed. In summary, friction heat is a key factor in regulating the interface wear.

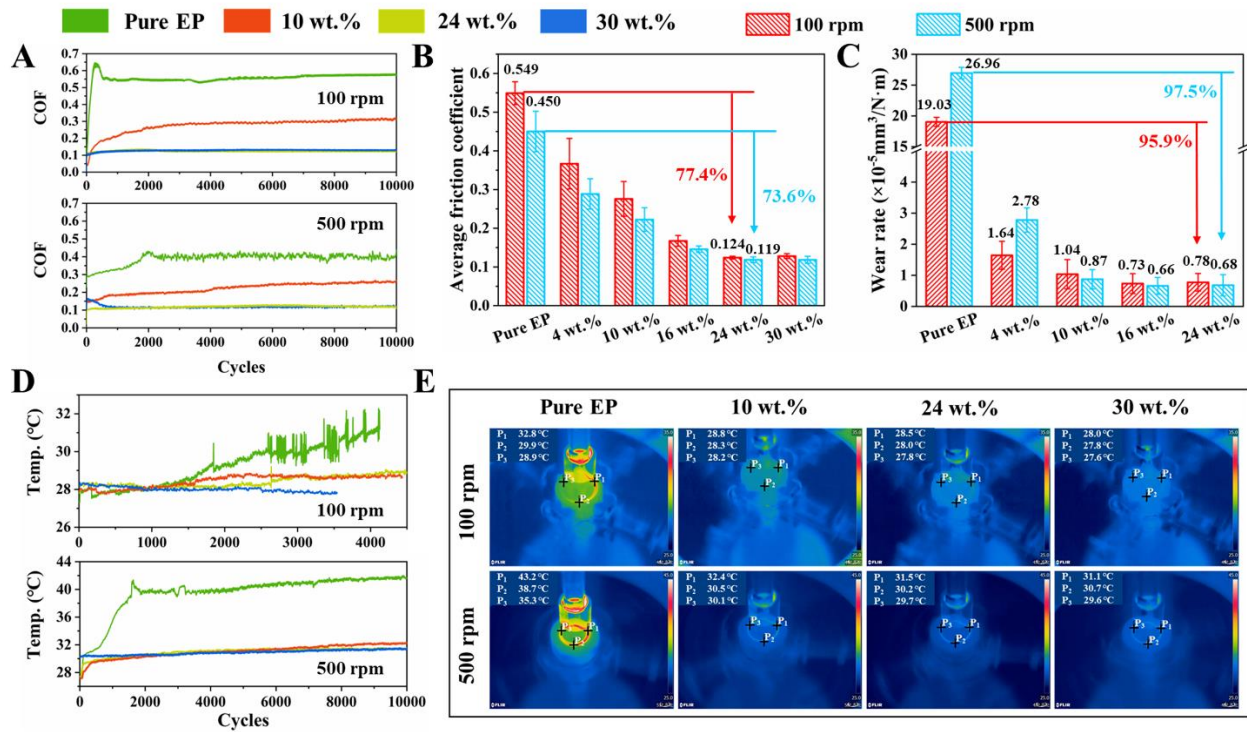


Fig. S8 Friction, wear, and infrared thermal imaging of EP and OD/EP coatings. (A) Variation of COFs with sliding cycles for the OD/EP coating at sliding speed of 100 rpm and 500 rpm. (B) Histogram of average friction coefficient in (A). (C) Pictures of wear rate of OD/EP coatings (the wear rate of OD/EP coatings with 30 wt.% cannot be calculated by WLI due to high surface roughness and slight wear). (D) Variation of temperature with sliding cycles for the OD/EP coating at sliding speed of 100 rpm and 500 rpm. (E) Pictures when the temperature of the wear track reaches stability in (D).

As shown in Fig. S9, the worn surface exhibits numerous furrows and severe wear when the OD content is less than 10 wt.%, which is due to the fact that the formed lubricant film is discontinuous.¹² With the OD content increases, the amount of liquid lubricant increases, forming

a continuous lubricant film. Then, the lubrication of the coating changes from boundary lubrication to film lubrication, which leads to light and smooth wear tracks.^{8,13}

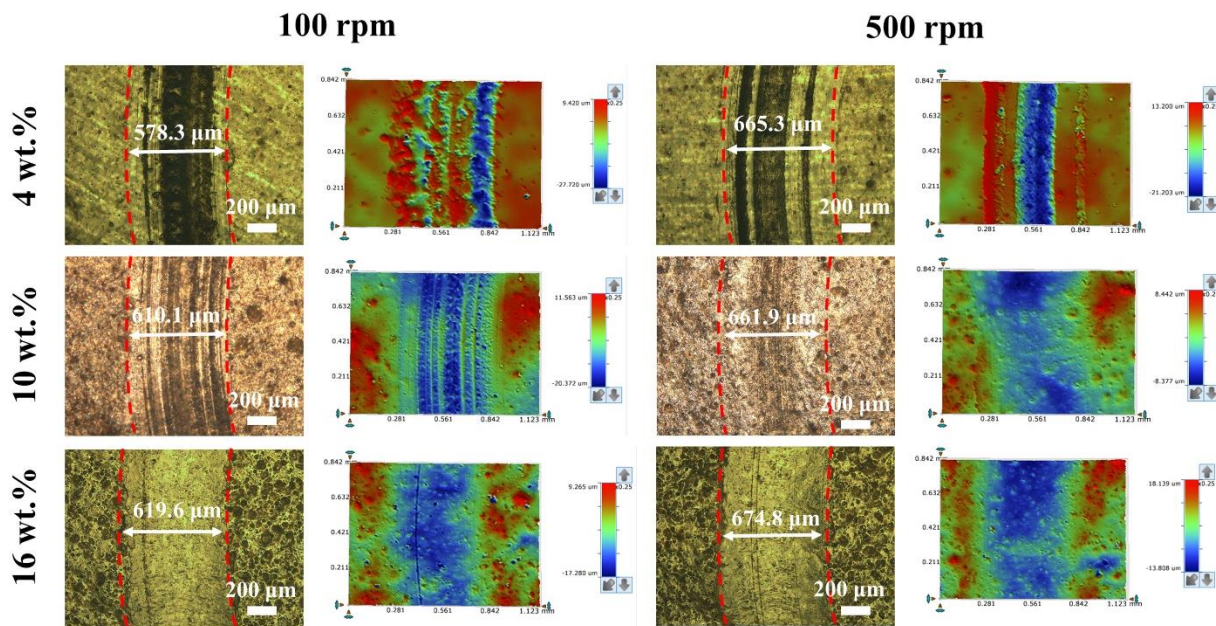


Fig. S9 Optical micrographs and 3D morphologies of OD/EP coatings with different OD contents were obtained under two friction test conditions.

The micrographs, 2D and 3D topographies of wear tracks for the pure EP and *n*-alkanols/EP coatings are showed in Fig. S10 and Fig. S11. The wear track on pure EP coating is relatively deep with obvious pits, spalling and adhesion points on the worn surface, indicating the fatigue and adhesive wear of the pure EP coating (Fig. S10).^{12,14} Due to the high stiffness and low toughness of the pure EP coating, fatigue wear is prone to occur and triggers the crack initiation and propagation under the shear stress.¹⁵ Meanwhile, because of the thermal effect of the high friction, the coatings is soften and plastic deformation, causing the adhesive wear.¹⁴ Obviously, for the *n*-alkanols/EP coatings, the depth and width of the wear tracks are slight, the fatigue wear is significantly suppressed (Fig. S10). This suggests the phase transition may minimize the degradation or thermal fatigue.¹⁶ Fig. S11 depicts the wear morphology of the counterpart steel balls, the wear scar of HD/EP coating is the slightest. Moreover, as compared to Pure EP coating, transfer film is visible on the wear scars surface of *n*-alkanols/EP coatings (Fig. S11). Therefore, the excellent tribological performance of *n*-alkanols/EP is ascribed to the synergistic effect of the low thermal effect and the lubricant films.

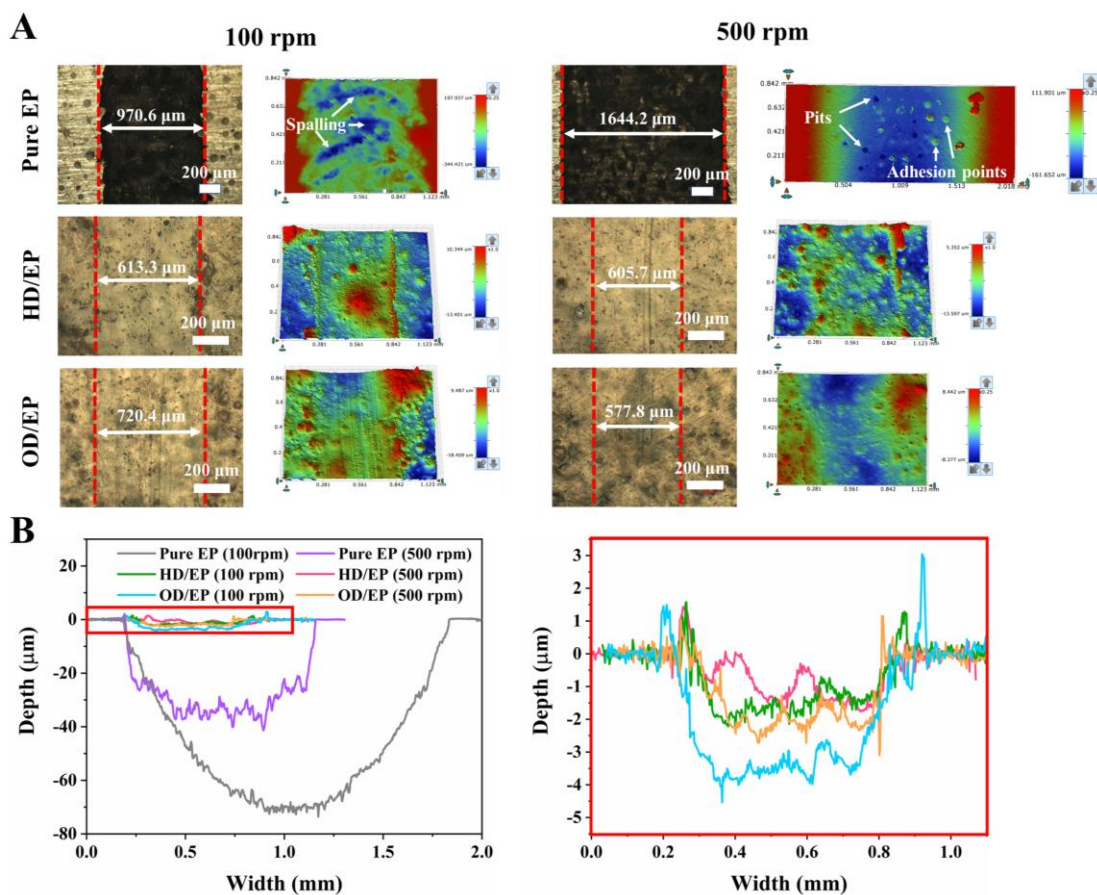


Fig. S10 Structure, 3D and 2D morphology of wear tracks. (A) Optical micrographs and 3D topographies of pure EP coating and *n*-alkanols/EP coatings under different sliding speeds. (B) 2D wear morphology of pure EP coating and *n*-alkanols/EP coatings under different sliding speeds. The depth and width of the wear tracks on *n*-alkanols/EP coatings are dramatically reduced. Among the *n*-alkanols/EP coatings, HD/EP coating has the smallest wear track width and depth (The 2D morphology of wear track on DS/EP coatings cannot be calculated by WLI due to high surface roughness and slight wear).

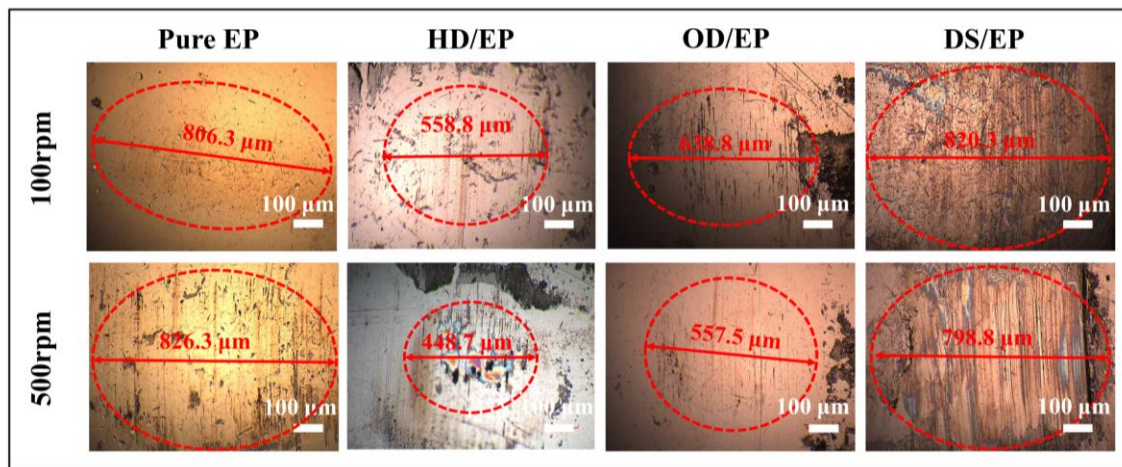


Fig. S11 Optical microscope pictures of wear scars of Pure EP and *n*-alkanols/EP composite coating. The wear scars of the pure EP coating are obviously scratched. The on the ball surface against the pure EP. There is a wax like transfer film on the wear scar of *n*-alkanols/EP coatings, and the wear scars of HD/EP coating are relatively smooth.

The hardness inside and outside the wear tracks were analyzed by Micro Vickers hardness tester (HV-1000), and the pressure was applied 0.25 N, the holding time was 15 s. In order to obtain reliable data, each type of coating was tested at least 3 times. The test results are shown in Fig. S12.

With the increase of OD content, the hardness inside and outside the wear track increase firstly and then decrease. When the OD content is 16 wt.%, the hardness reached the maximum. It is found that the general variation trend of coating hardness with the content is basically consistent with that of E' at room temperature, indicating that there is a good corresponding relationship between E' and hardness. Interestingly, when the content of OD is less than 16 wt.%, the hardness inside the wear tracks is greater than that outside the wear tracks. However, as the OD content further increases, the hardness inside the wear tracks becomes less than that outside the wear tracks. The variation in hardness is mainly due to the result of a pair of competition mechanisms. When the OD content is less than 16 wt.%, the coating is repeatedly rolled during the friction process, so that the hardness inside the wear track is greater than the hardness outside the wear track. With the OD content further increases, the lubricant is generated under the action of frictional heat and enriched in the wear track. The hardness of OD is lower compared to EP, so the hardness inside the wear track is lower than outside the wear track. Therefore, the variation of hardness inside and

outside the wear tracks also proves the solid-liquid phase transition of OD during friction, resulting in the generation of liquid lubricant within the wear track.

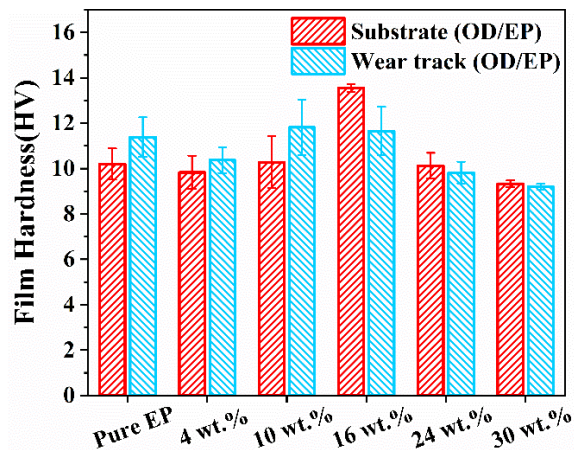


Fig. S12 Variation of micro-Vickers hardness for substrate and wear track of OD/EP coatings.

It can be seen from the Fig. S13 that the HD embedded in the EP is exposed to the contact area during the friction process, and the solid-liquid phase transition occurs under the induction of the friction heat, thus forming a lubricating layer at the friction interface. After the friction, the hexadecanol is exothermically solidified and then covers on the wear track surface.

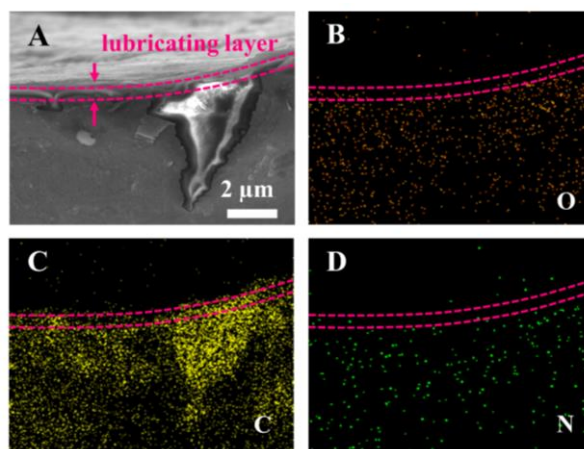


Fig. S13 SEM image of cross-section on wear track and EDS mapping image of corresponding elements. (A) SEM image of cross-section on wear track. (B-D) The cross-section of wear track corresponds to the element mapping of O, C, N.

A peak located at 2883 cm^{-1} is found in the Raman spectra of the wear track for OD/EP and DS/EP coatings (Fig. S14), which corresponds to the sharp peak of OD and DS, respectively. In addition, the Raman peaks of the wear scars for OD/EP and DS/EP coatings are basically consistent with OD and DS, respectively. As a result, it is established that the primary constituent of the lubricant films of OD/EP and DS/EP coatings are OD and DS, respectively.

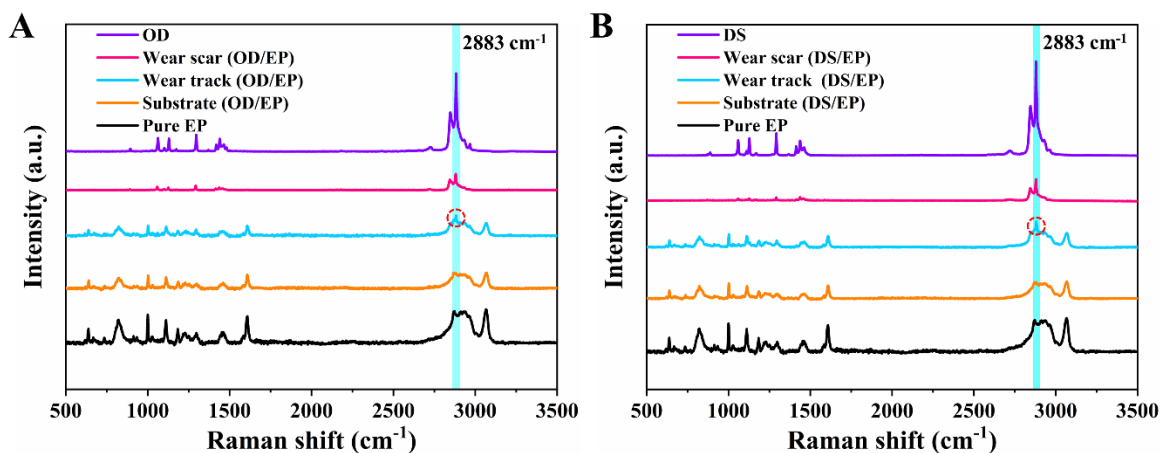


Fig. S14 Raman curves of the wear tracks and wear scars. (A) Raman analysis of wear track and wear scar of OD/EP coating. (B) Raman analysis of wear track and wear scar of DS/EP coating.

To further verify the effect of temperature on the tribological properties, we conducted a set of friction comparison experiments on pure EP and HD/EP coatings at room temperature (RT), $40\text{ }^{\circ}\text{C}$, $60\text{ }^{\circ}\text{C}$ and $80\text{ }^{\circ}\text{C}$, and pure EP coating with liquid HD under $60\text{ }^{\circ}\text{C}$ and $80\text{ }^{\circ}\text{C}$ respectively. The result is shown in Fig. S15, the friction coefficient and wear track width of pure EP firstly decrease with temperature, reaching the lowest value at $60\text{ }^{\circ}\text{C}$, then the friction coefficient increases as the temperature further increases to $80\text{ }^{\circ}\text{C}$. Moreover, many cracks are observed in the wear track at $80\text{ }^{\circ}\text{C}$. It is demonstrated that the rise of temperature led to the occurrence of softening and plastic deformation of the polymer coating, bringing severe damage. The test results of DMA showed that the storage modulus of the coating decreased gradually with the increased of temperature, indicating that the stiffness of the coating cut down, creating conditions for the deterioration of wear (Fig. S4).¹⁷ Therefore, increase the temperature can soften EP coating, decrease the brittleness of the EP coating, then decrease the friction coefficient and wear track width. However, further increase the temperature could badly bring the loss of mechanical properties of the coating, resulting in severe wear in the process of friction. The friction coefficient

of HD/EP coating is still lower than 0.15 even at the high temperature of 80 °C, and the wear track is hard to find by optical microscope with only white marks below the wear track (Fig. S4B). The friction test of pure EP coating was conducted under liquid HD to investigate the effect of HD on the tribological performance of pure EP coating. In view of the relative high melting point of HD (49.5 °C, Table S1), the friction test was performance at 60 and 80 °C to ensure HD is in liquid state. The friction coefficient of the pure EP coating/liquid HD is significantly lower than that for pure EP coating, and the width of the wear track under 60 °C is slight while the wear track under 80 °C is even hard to observe. The results indicate that liquid HD is the key factor leading to outstanding lubrication property of pure EP coating.

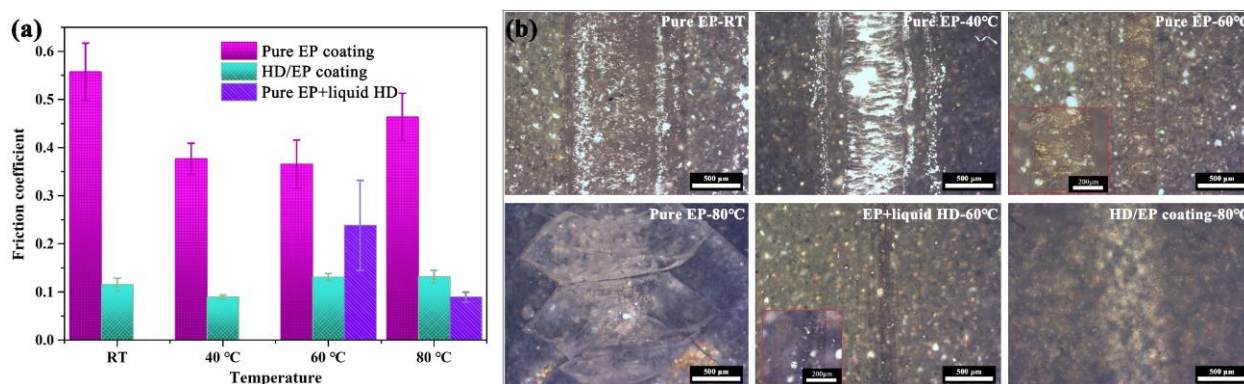


Fig. S15 Friction and wear of pure EP coating, HD/EP coating (16wt.% HD) and pure EP lubricated with liquid HD at different temperatures. (A) Friction coefficient of pure EP coating, HD/EP coating, and pure EP coating lubricated with liquid. (B) Optical microscope image of wear tracks for pure EP coating, HD/EP coating, and pure EP lubricated with liquid HD.

The smart lubricating material utilized the phase transition characteristics of *n*-alkanols and lubrication properties of liquid *n*-alkanols to significantly reduce the temperature of the friction interface, improving the tribological properties of the material. The data of friction and temperature fully verified the advantages of the smart lubricating material in temperature control and wear resistance.

REFERENCES

- 1 L. Veeramuthu, C.J. Cho, F.C. Liang, M. Venkatesan, R. Kumar G, H.Y. Hsu, R.J. Chung, C.H. Lee, W.Y. Lee and C.C. Kuo, *ACS Appl. Mater. Interfaces*, 2022, 14, 30160
- 2 K. Yang, J. Guan, K. Numata, C. Wu, S. Wu, Z. Shao and R. O. Ritchie, *Nat. Commun.* 2019, **10**,

3786.

- 3 B. Wu, Y. Jiang, Y. Wang, C. Zhou, X. Zhang and J. Lei, *Int. J. Heat. Mass. Transfer.* 2018, **126**, 1134.
- 4 Q. Feng, J. Yang, Y. Liu, H. Xiao and S. Fu, *J. Mater. Sci. Technol.* 2014, **30**, 1.
- 5 Q. Lin, X. Wang, M. Cai, H. Yan, Z. Zhao, X. Fan and M. Zhu, *Appl. Surf. Sci.* 2021, **568**, 150938.
- 6 F. Liu, Z. Shi and Y. Dong, *Compos. Part. A Appl. S.* 2018, **112**, 337.
- 7 S. Sundararajan, A. Kumar, B. C. Chakraborty, A. B. Samui and P. S. Kulkarni, *Sustain. Energ. Fuels.* 2018, **2**, 688.
- 8 C. Yu, P. Ju, H. Wan, L. Chen, H. Li, H. Zhou and J. Chen, *Prog. Org. Coat.* 2020, **145**, 105667.
- 9 A. Bejan, *Advances in Heat Transfer* 1994, **24**, 1.
- 10 X. Li, Y. Ling, G. Zhang, Y. Yin, Y. Dai, C. Zhang and J. Luo, *Compos. Part. B Eng.* 2020, **196**, 108133.
- 11 H. Yan, L. Zhang, H. Li, X. Fan and M. Zhu, *Carbon* 2020, **157**, 217.
- 12 S. T. Pham, A. K. Tieu, V. Sencadas, W. Lei, D. Liu, S. Wan and J. Hao, *ACS Appl. Mater. Interfaces.* 2021, **13**, 7714-7724.
- 13 L. Zhang, G. Xie, S. Wu, S. Peng, X. Zhang, D. Guo, S. Wen and J. Luo, *Friction* 2019, **9**, 29.
- 14 R. Aghababaei, D. H. Warner, and J. F. Molinari, *Nat. Commun.*, 2016, **7**, 11816.
- 15 J. Kim, G. Zhang, M. Shi and Z. Suo, *Science*, 2021, **374**, 212-216.
- 16 S. Sundararajan, A. Kumar, B. C. Chakraborty, A. B. Samui and P. S. Kulkarni, *Sustain. Energ. Fuels*, 2018, **2**, 688-697.
- 17 C. Liu, Z. Li, W. Lu, Y. Bao, W. Xia, X. Wu, H. Zhao, B. Gault, C. Liu, M. Herbig, A. Fischer, G. Dehm, G. Wu and D. Raabe, *Nat. Commun.*, 2021, **12**, 5518.